# Absolute entropy and free energy of fluids using the hypothetical scanning method. I. Calculation of transition probabilities from local grand canonical partition functions

Agnieszka Szarecka, Ronald P. White, and Hagai Meirovitch[a)]
*Center for Computational Biology and Bioinformatics, and Department of Molecular Genetics and Biochemistry, University of Pittsburgh School of Medicine, W1058 BST, Pittsburgh, Pennsylvania 15261*

(Received 1 August 2003; accepted 22 September 2003)

The hypothetical scanning (HS) method provides the *absolute* entropy and free energy from a Boltzmann sample generated by Monte Carlo, molecular dynamics or any other exact simulation procedure. Thus far HS has been applied successfully to magnetic and polymer chain models; in this paper and the following one it is extended to fluid systems by treating a Lennard-Jones model of argon. With HS a probability $P_i$ approximating the Boltzmann probability of system configuration $i$ is calculated with a stepwise reconstruction procedure, based on adding atoms gradually layer-by-layer to an initially empty volume, where they are replaced in their positions at $i$. At each step a transition probability (TP) is obtained from local grand canonical partition functions calculated over a limited space of the still unvisited (future) volume, the larger this space the better the approximation. $P_i$ is the product of the step TPs, where $\ln P_i$ is an upper bound of the *absolute* entropy, which leads to upper and lower bounds for the free energy. We demonstrate that very good results for the entropy and the free energy can be obtained for a wide range of densities of the argon system by calculating TPs that are based on only a very limited future volume.  [DOI: 10.1063/1.1625919]

## I. INTRODUCTION

Calculation of the *absolute* entropy $S$ and the Helmholtz free energy $F$ of complex many-body systems by computer simulation is an extremely difficult problem that has been given considerable attention (see Refs. 1–4, and references cited therein). Using any simulation technique, it is relatively easy to calculate the energy, $E_i$, which is ''written'' on system configuration $i$ in terms of microscopic interactions (e.g., Lennard-Jones interactions of argon), and for the same reason to calculate structural quantities such as the radial distribution function of a fluid, or the radius of gyration of a polymer. On the other hand, calculating $S \sim -\ln P_i^B$ requires knowledge of the *value* of the Boltzmann probability, $P_i^B$, which is the sampling probability. However, $P_i^B$ is not provided directly by the commonly used *dynamical* techniques, the Metropolis Monte Carlo (MC)[5] method and molecular dynamics (MD);[6,7] therefore, at an absolute temperature $T$, $F=E-TS$ is unknown as well. For some models, e.g., a protein in vacuum, this problem can somewhat be alleviated by treating a microstate (i.e., the local MD or MC fluctuations around a stable conformation such as the $\alpha$-helix) by harmonic or quasiharmonic approximations, meaning that $P^B$ is assumed to be Gaussian.[8–15] In most cases, however, the commonly used methods for calculating $F$ and $S$ are based on reversible thermodynamic integration over physical quantities such as the energy, temperature, pressure, and the specific heat, as well as nonphysical parameters[1–4,16–27] (free energy perturbation methods, histogram analysis methods,[28,29] and other related techniques[30–34] are also included in this category). Thermodynamic integration (TI) methods provide the difference in the free energy, $\Delta F_{m,n}$ (and in some cases $\Delta S_{m,n}$) between two microstates $m$ and $n$, and only when the absolute entropy of one microstate is known can that of the other be obtained.

While TI is a robust approach that has been applied successfully to highly complex systems, difficulties arise when the integration path includes a phase transition; also, for proteins, for example, such integration is feasible only if the structural variance between the two microstates is very small. Therefore, it is important to develop methods that provide $\ln P_i$, thereby enabling one to calculate the absolute $F_m$ and $F_n$ from two separate simulations of the microstates $m$ and $n$; in this case $\Delta F_{m,n}=F_m-F_n$ can be calculated even for *significantly different* microstates since the integration process is avoided.

Such an approach has been proposed by Meirovitch, where two related approximate techniques, the local states method[4,35–40] (see also Refs. 41–45) and the hypothetical scanning (HS) method[4,46–51] have been developed and applied to a wide range of systems, magnets, polymer chains, peptides, and loops in proteins. These methods demonstrate that like the energy, $\ln P_i$ is also ''written'' on system configuration $i$ in terms of a product of transition probabilities (TPs), where each method provides a different prescription for the ''reading'' of these TPs from $i$. Thus, the absolute entropy, like the energy, can be obtained approximately from a given Boltzmann sample generated by MC or MD (or any other exact method), even in cases where TI is practically unfeasible.

a)Author to whom correspondence should be addressed.

 

Our long-range objective is to extend these methods to a protein immersed in a box of explicit solvent (water); however, none of them have been applied thus far to a continuum fluid model. Therefore, in this paper and the following one we extend the HS method to a Lennard-Jones model of liquid argon, because HS was found to be significantly more efficient than the local states method for treating the molecular van der Waals repulsions in a dense environment. With HS a probability $P_i$ approximating the Boltzmann probability of system configuration $i$ is calculated by a reconstruction procedure based on adding atoms gradually to an initially empty volume, where they are placed in their positions at $i$; in this process the volume is divided into small cells which are visited in a *linear* order, line-by-line, layer-by-layer. At each step a TP is obtained by systematically calculating local grand canonical partition functions over a limited space of the still unvisited (future) volume. $P_i$ is the product of the step TPs, where $\ln P_i$ estimates the *absolute* entropy that leads to upper and lower bounds for the free energy.

For simplicity, before treating argon, we describe HS as applied to the square Ising lattice, where the effect of the boundary conditions is discussed in detail. Then, a grand canonical future scanning for calculating the TPs of argon is discussed, and the HS results are compared to those obtained by using an efficient TI technique. In the following paper the TPs are calculated in an alternative way, by a counting procedure based on Metropolis MC simulations within the framework of the canonical ensemble.

## II. THEORY AND METHODS

To understand the theory of HS for a continuum fluid it proves convenient to introduce it first in terms of the square Ising lattice, which is equivalent to a lattice gas model of a fluid. The Ising model consists of $N=L\times L$ spins $\sigma_k$, $\sigma_k=\pm 1$ $(1\leqslant k\leqslant N)$, where nearest neighbor spins at $k$ and $l$ interact with ferromagnetic energy $-J\sigma_k\sigma_l$ $(J>0)$. The total energy of system configuration $i$ is denoted by $E_i$ and the Boltzmann probability of $i$, $P_i^B$ is

$$P_i^B=\frac{\exp-[E_i/k_BT]}{Z}, \tag{1}$$

where $T$ is the absolute temperature, $k_B$ is the Boltzmann constant, and $Z$ is the partition function. The ensemble average $\langle E\rangle$ of the energy is

$$\langle E\rangle=\sum_i P_i^B E_i, \tag{2}$$

and the entropy and the free energy can formally be expressed as ensemble averages, $\langle S\rangle$ and $\langle F\rangle$ but we shall denote them in the usual way by $S$ and $F$, respectively,

$$S=\langle S\rangle=-k_B\sum_i P_i^B \ln P_i^B \tag{3}$$

and

$$F=\langle F\rangle=\sum_i P_i^B[E_i+k_BT\ln P_i^B]=\langle E\rangle-TS. \tag{4}$$

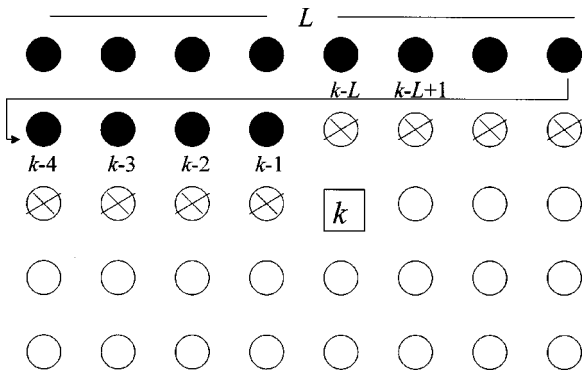


FIG. 1. A diagram illustrating the $k$th step of the DS construction (or HS reconstruction) of a square Ising lattice of $L\times L$ spins. The target site $k$ is denoted by a square and the $L$ "uncovered" spins (at sites $k-L$, $k-L+1$,...,$k-2$, $k-1$) are denoted by empty circles with two crossing lines. In addition to the "uncovered sites," the full circles denote lattice sites which have also been filled with spins $(\pm 1)$ in previous steps of the construction process, while the empty circles denote the still empty lattice sites. The future partition functions, $Z^+(k)$ and $Z^-(k)$ for $\sigma_k=+1$ and $-1$, respectively, are calculated from the configurations of the $2^{10}$ future spins defined over the 10-site rectangle; notice that the interaction energy between the uncovered spins at sites, $k-1$, $k-2$, $k-L$, and $k-L+1$ and their nearest neighbor future spins is considered. The "spiral" boundary conditions between spin $L$ and spin 1 of the next row is depicted by an arrowed line (In other words, we imagine spin $L$ to be placed to the left of spin 1 when calculating spin 1's interactions). The TPs are $p^+=Z^+/(Z^++Z^-)$ and $p^-=(1-p^+)$.

This model can straightforwardly be simulated by the usual Metropolis MC method, where one starts from an arbitrary spin configuration, changes it gradually in the course of the run, and calculates averages of properties of interest after the system has been equilibrated. Alternatively, this system has been viewed by Alexandrowicz[52,53] (see also Kikuchi[54]) as a long *linear* chain of spins that can be constructed by adding spins to an initially empty lattice step-by-step with the help of approximate transition probabilities (TPs). A related method, called direct scanning (DS) was suggested later by Meirovitch,[55] where a set of approximate TPs, is obtained by scanning *future* spin configurations on $f$ empty lattice sites close to the target site (see below), where the approximation can be improved systematically by increasing $f$. This DS procedure is the basis of the HS method and therefore is described below in detail.

### A. The DS procedure

With the DS procedure, one starts from an $N=L\times L$ *empty* lattice, and determines the spins step-by-step, row-by-row using TPs. At step $k$ of the process, $k-1$ spins have already been fixed and one seeks to determine the spin at the vacant site $k$ (the "target" site). The last $L$ spins added to the lattice are called the "uncovered" spins (see Fig. 1). Because of the nearest neighbor interaction, the TPs depend on these $L$ uncovered spins, but not on the covered ones (i.e., spins 1 to $k-L-1$, which were determined in the past, see Fig. 1), where the effect of an uncovered spin is expected to decrease as its distance from site $k$ increases. The *exact* TP at step $k$ would require calculating two partition functions, $Z^+(k)$ and $Z^-(k)$ over the *empty* part of the lattice [the $N-(k-1)$ still vacant sites, $k$, $k+1$,...,$N$], where site $k$ is populated by a

spin $+1$ or $-1$, respectively; the corresponding TPs are $Z^+(k)/[Z^+(k)+Z^-(k)]$ and $Z^-(k)/[Z^+(k)+Z^-(k)]$. These partition functions are based on summation of the energy exponentials of all the possible spin configurations over the vacant sites in the presence of the (fixed) configuration of the uncovered spins. That is, interaction energies between vacant sites and the fixed uncovered spins are also taken into account. In this respect determination of spin $k$ always depends on the past, i.e., the previously determined $L$ spins $k-1,...,k-L$. In practice, this calculation is not feasible for a large lattice and one can calculate $Z^+$ and $Z^-$ only approximately over a limited rectangular part of the empty lattice consisting of $f$ empty sites, such as the ten empty sites appearing in the rectangle in Fig. 1; the corresponding approximate TPs, are denoted $p_k(\pm,f,\alpha)$, where $\alpha$ is a set of parameters (discussed later) that are optimized by a minimum free energy criterion,

$$p_k(+,f,\alpha)=\frac{Z^+(k,f,\alpha)}{Z^+(k,f,\alpha)+Z^-(k,f,\alpha)}. \tag{5}$$

Using this method one can generate a sample of *statistically independent* Ising configurations, where in contrast to the MC method, the *value* of the construction probability of configuration $i$ is known,

$$P_i(f,\alpha)=\prod_{k=1}^{N} p_k(f,\alpha), \tag{6}$$

where $p_k(f,\alpha)$ is the TP of the spin selected at site $k$. Therefore, the absolute entropy and free energy [Eqs. (3) and (4)] can be calculated and very good approximations for these quantities indeed have been obtained by the DS method.[55] {Notice that unlike the calculations carried out in Ref. 55, $Z$ can also be estimated by $\bar{Z}$ from a sample of size $n$ generated by $P_i(f,\alpha)$, where $\bar{Z}=1/n\Sigma_t^n \exp[-E_t/k_BT]/P_t(f,\alpha)$.}

### B. Treatment of the boundaries

To maintain a *linear* construction, the natural treatment of the boundaries with the DS procedure is by imposing ''spiral'' boundary conditions. Thus, the first spin of a row becomes a nearest neighbor to the last spin of the previous row, i.e., these are interacting spins (see Fig. 1). This definition leads to a ''homogeneous'' set of TPs, i.e., TPs that are defined exactly the same for internal and boundary spins. Still, this procedure is not completely homogeneous, because when the last row is approached the size of the rectangle of future spins should be decreased to remain within the limits of the lattice; also, the first row is not ''neighbored'' by a previous row, which requires defining a particular set of TPs for the first row. These spins can be chosen in various ways, where a simple one is to select them independently at random $[p(+)=p(-)=0.5]$, or with $p(+)=(m+1)/2$ if the magnetization $m$ is known (at least approximately). Notice that with such choices the probability $P_i(f,\alpha)$ [Eq. (6)] is well defined over the entire system of $2^N$ configurations, i.e., $\Sigma P_i(f,\alpha)=1$; these boundary conditions are denoted BC1.

As discussed below, defining homogeneous boundary conditions simplifies the programming immensely, especially for a continuum 3D model; furthermore, for a large enough system their effect becomes negligible. Thus, to define a completely homogeneous set of TPs, suppose that a rectangular (rather than square) Ising ''superlattice'' of $KL\times L$ spins (i.e., of $K$ successive *square* Ising lattices of $L\times L$ spins) has been generated by DS with spiral boundary conditions, and let us examine the middle lattices, say from lattice 2 to $K-1$. Obviously, with this construction the TPs for the first row are defined in the same way as for internal spins, because of the presence of the last row of spins of the previous square lattice. Also, the rectangle of future spins (see Fig. 1) is not changed for the last rows of each square lattice, because if needed it is defined also over sites of the next square lattice (i.e., the future is open). Thus, the probability of a square Ising lattice generated with this procedure is $p_{\mathrm{row}}P_i(f,\alpha)$, where $p_{\mathrm{row}}$ is a DS probability of the last row of the previously generated lattice. Because the energy of interaction between the first and last rows of successive lattices is calculated the total number of spin–spin interactions is $2N$, as for periodic boundary conditions (see discussion below), and the related entropy is $\sim -k_B \ln P_i(f,\alpha)$. These boundary conditions,[55] denoted BC2, can be extended to an Ising model on a simple cubic lattice as well, by adding the spins layer-by-layer where for each layer they are added row-by-row as described above.

The homogeneous BC2 boundary conditions described above for DS are not the commonly used boundary conditions. Typically the Ising model is studied with periodic boundary conditions, where row 1 interacts with the last row, $L$, and the first and last spins at each row interact as well. In practice one defines image lattices where rows 0, $-1$, $-2$, etc. are the images of rows $L$, $L-1$, and $L-2$, respectively, and similar images are defined for columns 1 and $L$. Clearly, constructing by DS an Ising lattice with periodic boundary conditions is very inconvenient because of the need to define a special set TPs for the boundaries. For example, since row 1 interacts with both rows 2 and 0, the immediate future of row 1 is defined not only by vacant sites of say, rows 2, 3, and 4, but also by the symmetrical sites on rows 0, $-1$, and $-2$ that are the images of rows $L$, $L-1$, and $L-2$, respectively. This means that to treat row 1 on the same level of approximation as applied to internal spins, the number of future sites considered should be at least $2f$ rather than $f$; for the same reason, $2f$ future sites are also required for calculating the TP of the first spin of each row. On the other hand, for rows close to the last row, $L$ one should consider the interaction energy of the future spins with the image row $L+1$, which is defined by the already constructed row 1. Similarly, for each row, calculating TPs for spins that are close to the end site, $L$, requires considering the image spin $L+1$, which is defined by the already constructed spin 1 of the same row. In practice, treating $2f$ spins can be computationally undesirable and the number of different cases to be considered is large, becoming significantly larger for three-dimensional models, which makes the programming cumbersome. Approximate implementation of periodic boundary conditions within the framework of DS is called BC3.

As pointed out earlier, for *large* systems the effect of the

boundaries becomes negligible and DS with different boundary conditions will lead practically to the same results. However, it is much easier to program a DS procedure based on the homogeneous TPs(BC2) than on the inhomogeneous TPs(BC3), especially when boundary effects are complex, e.g., for three-dimensional systems and models that depend on long-range interactions and strong repulsions, as the Lennard-Jones model for argon, studied in the present paper.

### C. The HS method

One can simulate a *large* square Ising lattice by DS or alternatively by the Metropolis MC method with periodic boundary conditions. If the temperature $T$ is not too close to the critical temperature and the future scanning is based on a rectangular box larger than the correlation length, statistical averages and fluctuations of various quantities such as the energy, entropy, or magnetization obtained from the two samples would be the same within the statistical error, because the effect of the boundaries is negligible.[55] In this respect the two samples are equivalent and independent of the methods used to generate them; notice, however, that DS, unlike MC also provides the absolute entropy.

The HS method (and the local states method not discussed here) enables one to calculate the entropy of a sample generated by *any* exact procedure, in particular the MC method. Thus, relying on the above equivalence, one assumes that the MC sample has rather been constructed by DS, which allows reconstructing the TPs that *hypothetically* were used to build configuration $i$ with DS. In practice, one starts from an empty lattice, and at each step $k$ calculates $Z^+(f,\alpha)$ and $Z^-(f,\alpha)$ from which $p_k(f,\alpha)$ [Eq. (5)] for the *actual* spin appearing at this site in configuration $i$ is obtained. The product of these TPs leads to $P_i(f,\alpha)$ [Eq. (6)] and to the corresponding entropy functional $S^A(f,\alpha)$. One can show that $S^A$ is a rigorous upper bound for the correct entropy,[48] and $F^A(f,\alpha)$ is therefore a lower bound free energy functional,

$$S^A(f,\alpha) = -k_B \sum_i P_i^B \ln P_i(f,\alpha); \tag{7}$$

$$F^A(f,\alpha) = \langle E \rangle - TS^A(f,\alpha). \tag{8}$$

Notice that $S^A$ and $F^A$, like $\langle E \rangle$, $S$ and $F$ in Eqs. (2), (3), and (4), respectively, are defined over the *entire* ensemble of $2^N$ Ising configurations; in practice $S^A$ and $F^A$ are *estimated* by $\overline{S^A}$ and $\overline{F^A}$ from a sample of size $n$ generated with an exact method such as the Metropolis method. For example, $\overline{S^A} = -(k_B/n)\Sigma_t^n \ln P_t(f,\alpha)$, where $t$ denotes the $t$th configuration in the sample. Thus, the entropy, like the energy, is ''written'' on the system configurations in terms of the logarithm of transition probabilities. The optimal values of the parameters $\alpha$ are those that minimize $S^A$ or maximize $F^A$.

Because the MC sample is typically generated with periodic boundary conditions, one option is to reconstruct the Ising configurations with the inhomogeneous set of TPs for these boundaries defined earlier as BC3, or the more homogeneous set of TPs (that include the spiral connections) denoted BC1. However, we describe now an additional set of boundaries denoted BC4 that lead to a completely homogeneous set of TPs for HS. Thus, row 1 is reconstructed in the presence of image row 0 defined by the *known* spin configuration of row $L$. Likewise, to reconstruct spin 1 of any row $j$, the image spins at sites 0, $-1$, $-2$, etc. of row $j$ (defined by the *known* spins at sites $L$, $L-1$, $L-2$, etc. of row $j$, respectively) are considered for calculating the required TP. On the other hand, for reconstructing the last spins of row $j$ (say, at sites $L-3$, $L-2$, $L-1$, and $L$), the image spins of this row at sites $L+1$, $L+2$, etc. are not considered, i.e., these sites are treated as vacant, as for BC2; thus, when the spins in the last sites of row $j$ are reconstructed the corresponding rectangles are defined partially over sites that pertain to image columns $L+1$, $L+2$, etc. that are not part of the $L \times L$ lattice. Likewise, image spins in rows $L+1,\ldots,2L$ are ignored, i.e., these sites remain vacant; therefore, the same rectangle of future spins for calculating the TPs is used for all the rows, where for the last rows part of this rectangle is defined over future sites of rows $L+1$ and higher, again as in BC2; see Fig. 2.

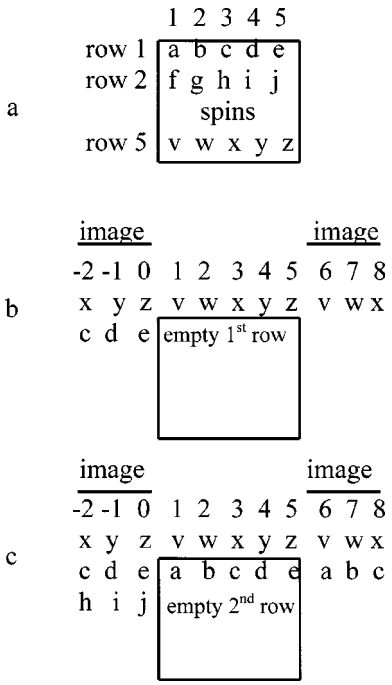


FIG. 2. The BC4 boundary conditions for a square Ising model. (a) A $5\times5$ Ising lattice where the spins of the first, second, and last rows are specified by letters. (b) The periodic boundary conditions used to reconstruct the first row of this lattice. Notice that this row remains open to the right throughout its construction process. (c) Upon completion of the first row, ''right-hand'' images (a, b, and c) are then added and used for the reconstruction of the second row; also added at the beginning of the reconstruction of the second row are the ''left-hand'' images (h, i, and j). The boundaries and the reconstruction of the other rows is similar; note, however, for the last rows the rectangle of future spins (see Fig. 1) if necessary might also be defined over the continuing rows 6, 7, etc., i.e., the lattice is open ''below'' (and ''to the right'' in the current row).

It should be pointed out that BC4 differs conceptually from BC1, BC2, and BC3 in that the HS reconstruction at the boundaries does not depend only on spins that were reconstructed in the past but also on the images of spins that will be determined in future steps of the HS process. However, these future spins are used to define a homogeneous environment for calculating the TPs of spins close and at the boundaries; in this respect each spin on the lattice is reconstructed

under exactly the same rules, which characterizes to a great extent the situation in a very large system. In principle, these future boundary spins could be replaced by any set of spins that are distributed according to the Boltzmann probability.[56] Again, for a large system, the effect of the BC4 boundary conditions vanishes. BC4 is found to be very useful for a continuum model of argon, where the effect of the atomic repulsions is strong, while such repulsions do not exist at all in the Ising model.

### D. Upper bounds for the free energy

One can define another approximate free energy functional denoted $F^B(f,\alpha)$ (Ref. 48) [$F^B$ is defined over the whole ensemble, see discussion following Eqs. (7) and (8)],

$$F^B(f,\alpha)=\sum_i P_i(f,\alpha)[E_i+k_BT\ln P_i(f,\alpha)], \tag{9}$$

where according to the free energy minimum principle,[57] $F^B(f,\alpha)\geqslant F$ [Eq. (4)] and equality occurs when $P_i(f,\alpha)=P_i^B$ [Eq. (1)]; $F^B(f,\alpha)$, the upper bound of $F$, can be *estimated* by $\overline{F^B}$ from a sample of size $n$ generated with $P_i^B$, using importance sampling,

$$\overline{F^B}(f,\alpha)=\frac{\Sigma_{t=1}^n P_t(f,\alpha)\exp[E_t/k_BT][E_t+k_BT\ln P_t(f,\alpha)]}{\Sigma_{t=1}^n P_t(f,\alpha)\exp[E_t/k_BT]}, \tag{10}$$

where $t$ denotes the $t$th configuration in the sample obtained with a *correct* Boltzmann simulation carried out with the MC or MD methods, for example. (The factors $1/n$ in the numerator and the denominator are canceled.) However, the statistical reliability of this estimation (unlike the estimation of $F^A$) decreases sharply with increasing system size, because the overlap between the probability distributions $P_i^B$ and $P_i(f,\alpha)$ decreases exponentially (see discussion in Ref. 39).

Another way to estimate $F^B(f,\alpha)$ is by using a "reversed Schmidt procedure,"[39,48] which enables one to extract from the given *unbiased* sample of size $n$ generated with $P_i^B$ an effectively smaller *biased* sample generated with $P_i(f,\alpha)$. Thus, the configurations of the unbiased sample are treated consecutively. If a configuration $i$ was accepted to the biased sample, the next configuration $j$ would be accepted with a transition probability $A_{ij}$,

$$A_{ij}=\min\{1,\exp[(E_j-E_i)/k_BT]P_j(f,\alpha)/P_i(f,\alpha)\}. \tag{11}$$

Equation (11) is a generalized MC procedure, which satisfies the detailed balance condition and is carried out with random numbers. The acceptance rate $R$ provides a measure for the *effective size* of the accepted biased sample,

$$R=n_{\text{accept}}/n, \tag{12}$$

where $n_{\text{accept}}$ is the number of accepted configurations.

Given that $F^A(f,\alpha)$ and $F^B(f,\alpha)$, are calculated and their deviations from $F$ (in the absolute values) are approximately equal, their average $F^{M1}(f,\alpha)$ becomes a better approximation than either of them individually,

$$F^{M1}(f,\alpha)=[F^A(f,\alpha)+F^B(f,\alpha)]/2. \tag{13}$$

Typically, several approximations for $F^A(f,\alpha)$, $F^B(f,\alpha)$, and $F^{M1}(f,\alpha)$ are calculated as a function of $f$, and their convergence enables one to determine the correct free energy with high accuracy.

### E. The correlation between $\sigma^A(f,\alpha)$ and $F^A(f,\alpha)$

The fluctuation (standard deviation) $\sigma$ of the *correct* free energy, $F$, [Eq. (4)] is zero, while $F^A(f,\alpha)$ has nonzero fluctuation, $\sigma^A$,[46,51,58]

$$\sigma^A=\left[\sum_i P_i^B[F_i^A(f,\alpha)]^2-\left(\sum_i P_i^B F_i^A(f,\alpha)\right)^2\right]^{1/2}. \tag{14}$$

For a good enough approximation $\sigma^A$ is expected to decrease as the approximation improves. It has been suggested[46] to express the correlation between $F^A(f,\alpha)$ and $\sigma^A(f,\alpha)$ by the approximate function,

$$F^A(f,\alpha)=F^{\text{extp}}+C[\sigma^A(f,\alpha)]^\beta, \tag{15}$$

where $F^{\text{extp}}$ is the extrapolated value of the free energy, and $C$ and $\beta$ are parameters to be optimized by best-fitting results for $F^A(f,\alpha)$ and $\sigma^A(f,\alpha)$ for different $f$. One can also calculate the tangent to the function at the lowest value obtained for $\sigma^A(f,\alpha)$; if Eq. (15) defines a concave-down function and this trend of $F^A(\sigma^A)$ is assumed to hold for better (uncalculated) approximations $F^A$, the intersection of the tangent with the vertical axis [$\sigma^A(f,\alpha)=0$] defines an upper bound for $F$ denoted $F^{\text{up}}(f,\alpha)$ that depends on the largest value of $f$ used in the best-fit process. Thus, in parallel to Eq. (13), one defines the average, $F^{M2}(f,\alpha)$,

$$F^{M2}(f,\alpha)=[F^A(f,\alpha)+F^{\text{up}}(f,\alpha)]/2. \tag{16}$$

### F. The model of argon

In this paper we extend HS to a system of $N$ atoms contained in a 3D "box" of volume $V$ [($NVT$) ensemble] interacting via a Lennard-Jones potential (argon atoms),

$$\phi(r)=4\epsilon\left[\left(\frac{\sigma}{r}\right)^{12}-\left(\frac{\sigma}{r}\right)^{6}\right], \tag{17}$$

where $r$ (in Å) is the distance between a pair of atoms, $\epsilon/k_B=119.8$ K and $\sigma=3.405$ Å. Denoting the Cartesian coordinates and their differentials by $\mathbf{x}^N$ and $d\mathbf{x}^N$, respectively, the *configurational* Boltzmann probability density $\rho(\mathbf{x}^N)$ is

$$\rho(\mathbf{x}^N)=\exp[-E(\mathbf{x}^N)/k_BT]/Z_N$$
$$=\exp[-E(\mathbf{x}^N)/k_BT]/\int_\Omega \exp[-E(\mathbf{x}^N)/k_BT]d\mathbf{x}^N, \tag{18}$$

where $\Omega=V^N$ and $E(\mathbf{x}^N)=\Sigma_{i<j}\phi(r_{ij})$ is the potential energy. The total entropy $S$ is

$$S=S_{\text{IG}}+S_e=S_{\text{IG}}-k_B\int_\Omega \rho(\mathbf{x}^N)\ln[V^N\rho(\mathbf{x}^N)]d\mathbf{x}^N, \tag{19}$$

where $S_{\text{IG}}$ is the entropy of the ideal gas at the same temperature and density, and $S_e$ is the excess entropy to be estimated by HS. The corresponding excess Helmholtz free energy is,

$$F_e = \int_\Omega \rho(\mathbf{x}^N) E(\mathbf{x}^N) d\mathbf{x}^N - TS_e = E - TS_e, \tag{20}$$

where $E$ is the average potential energy. However, to compare our results to those obtained by other methods we shall also calculate the configurational free energy, denoted $A_c$,[26]

$$A_c = -k_B T \ln\left(\frac{Z_N}{N!\sigma^{3N}}\right), \tag{21}$$

where the partition function $Z_N$ is defined in Eq. (18).

### G. The HS method applied to argon

This system was simulated by the Metropolis MC method and the free energy and entropy were calculated with HS from the corresponding samples. Conforming with the equivalence of the Ising and the lattice gas models ($+1$=an occupied site, $-1$=an unoccupied site), the box is divided into $L^3 = L\times L\times L$ cubic cells with the maximal size that still guarantees that no more than one center of a spherical argon molecule occupies a cell. However, to approximate the molecules in continuum each cell is further divided into $l = b \times b \times b$ subcells, called cubes. Notice that because the interaction is long-range, unlike for the Ising model, deeper layers than the uncovered layer should be considered in the calculation of the TPs.

Each sample configuration was reconstructed using HS, where at step $k$, $N_k$ atoms have already been treated and placed in their positions and the TP of the target cell ($k$) (which might be an occupied or an unoccupied cell) should be determined. An *exact* TP will require calculating the two *canonical* partition functions, $Z^+(k)$ and $Z^-(k)$ (defined for the present continuum model) for the remaining $N-N_k$ atoms distributed in the $L^3-(k-1)$ remaining cells. However, because only a limited number $f$ of future cells are considered, the population in these cells can range from 0 (all the $f$ cells are empty) to $\min(f, N-N_k)$. We define a *grand partition function*, $\Xi_f$, over the $f$ cells

$$\Xi_f(k) = 1 + Q_1(k)\exp[\mu/k_B T] + Q_2(k)\exp[2\mu/k_B T] + \cdots Q_f(k)\exp[f\mu/k_B T]. \tag{22}$$

$Q_d(k)$ is a canonical partition function of $d$ atoms occupying $f$ cells, and $\mu$ is a chemical potential. For example, $Q_1 = \Sigma_{i=1}^f Q_1^i$, where $Q_1^i$ (which will also be referred to as a "singlet") is a partition function of future cell $i$ ($i=1,f$) (from now on $k$ will be omitted in the definition of the partition functions $Q$),

$$Q_1^i = \frac{V_{\text{cube}}}{\Lambda^3} \sum_{m=1}^{l} \exp[-E_{m\text{-}env}/k_B T_p]. \tag{23}$$

In this equation $V_{\text{cube}}$ is the cube's volume, $\Lambda$ is the de Broglie wavelength, $(h^2/2\pi m k_B T)^{1/2}$, where $h$ is the Planck constant, and $m$ is the mass of the atom. $E_{m\text{-}env}$ is the energy of interaction of an imaginary atom placed at the center of cube $m$ of cell $i$ (unless an atom appears in $m$) with the already reconstructed $N_k$ atoms and the summation over the $l$ cubes approximates the integral $\int \exp[-E_{env}/k_B T_p] d\mathbf{x}$ over cell $i$; $T_p$ is a temperature parameter discussed below. When a real atom, i.e., an atom to be reconstructed, occupies cube $m$ of the target cell $k$, its coordinates are used for calculating $E_{m\text{-}env}$, rather than the center of the cube. Similarly, $Q_2$ is obtained as a sum over $f(f-1)/2$ "doublets" denoted $Q_2^{i,j}$, where

$$Q_2^{i,j} = \left(\frac{V_{\text{cube}}}{\Lambda^3}\right)^2 \sum_{m=1}^{l}\sum_{n=1}^{l} \exp[-(E_{m\text{-}env} + E_{n\text{-}env} + E_{m,n})/k_B T_p]. \tag{24}$$

In this equation $E_{m,n}$ is the interaction energy between imaginary atoms placed at the centers of cube $m$ of cell $i$ and cube $n$ of cell $j$. Correspondingly, for $d>2$, $Q_d$ is a summation over $f!/[(f-d)!d!]$ terms. The TP $P^+$ ($P^-$) for an occupied (unoccupied) target cell $k$, is proportional to the sum of the partition function terms that include (exclude) cell $k$. Thus, for the lowest approximation, where the only future cell is the target cell $k$ ($f=1$), $Q_1$ consists of one term, $\Xi_1 = 1 + Q_1 \exp[\mu/k_B T]$ and

$$P^+ = Q_1 \exp[\mu/k_B T]/\Xi_1, \quad P^- = 1 - P^+ = 1/\Xi_1. \tag{25}$$

However, in the case of an occupied target cell, unlike for the Ising model, one has to define the TP *density* $\rho^m$ for placing an atom at cube $m$,

$$\rho^m = P^+ \exp[-E_{m\text{-}env}/k_B T_p]/Q_1\Lambda^3 = \exp[-E_{m\text{-}env}/k_B T_p + \mu/k_B T]/\Xi_1\Lambda^3. \tag{26}$$

In the next approximation ($f=2$) the target cell (denoted 1) and an additional nearest neighbor future cell (denoted 2) are considered. One then calculates $Q_1 = Q_1^1 + Q_1^2$, $Q_2 = Q_2^{1,2}$, and $\Xi_2 = 1 + Q_1\exp[\mu/k_B T] + Q_2\exp[2\mu/k_B T]$, leading to

$$P^+ = Q_1^1 \exp[\mu/k_B T]/\Xi_2 + Q_2\exp[2\mu/k_B T]/\Xi_2,$$
$$P^- = 1 + Q_1^2 \exp[\mu/k_B T]/\Xi_2. \tag{27}$$

In the same way as above one can show that the TP density for placing an atom at cube $m$ of cell 1 (the target cell $k$) is $\rho^m = \rho_1^m + \rho_2^m$,

$$\rho_1^m = \exp[-E_{m\text{-}env}/k_B T_p + \mu/k_B T]/\Xi_2\Lambda^3$$
$$\rho_2^m = \exp[-E_{m\text{-}env}/k_B T_p + 2\mu/k_B T] \times \sum_{n=1}^{l} \exp[-(E_{n\text{-}env} + E_{m,n})/k_B T_p] V_{\text{cube}}/\Xi_2\Lambda^6. \tag{28}$$

Calculating the TPs for better approximations ($f>2$) is straightforward. Thus, the transition probability densities, $\rho^m$ and the transition probabilities for the empty cells, both denoted by $(\text{TP})_k$, are reconstructed for each configuration $i$ of the sample. Their product defines an approximate probability density, $\rho(\mathbf{x}^N, f, \alpha)$ over conformational space [compare with $P_i(f,\alpha)$, Eq. (6)],

$$\prod_k (\text{TP})_k = N!\,\rho(x^N, f, \alpha) \approx N!\,\frac{\exp[-E(x^N)/k_B T]}{Z_N}, \tag{29}$$

TABLE I. Densities, temperatures, and geometrical parameters for systems of $N=216$ atoms.[a]

| $\rho^*=N\sigma^3/V$ | $T^*=k_BT/\epsilon$ | $T$ (K) | Box length (Å) | $L$ | $L^3$ | $\rho_{\text{cell}}$ | Cell length (Å) |
|---|---|---|---|---|---|---|---|
| 0.846 | 0.806 | 96.53 | 21.6 | 9 | 729 | 0.296 | 2.40 |
| 0.75 | 1.15 | 137.77 | 22.49 | 9 | 729 | 0.296 | 2.50 |
| 0.5 | 1.35 | 161.73 | 25.74 | 11 | 1331 | 0.162 | 2.34 |
| 0.1 | 1.058 | 126.74 | 44.02 | 18 | 5832 | 0.037 | 2.45 |

[a]$V$, and $k_B$ are the volume and the Boltzmann constant, respectively. $\sigma$ and $\epsilon$ are the Lennard-Jones parameters [Eq. (17)], $\rho^*$ and $T^*$ are the reduced density and temperature, respectively, $L$ is the number of cells in each dimension, and $\rho_{\text{cell}}$ is $N/L^3$.

which yields the entropy functional $S^A$, using $\rho(\mathbf{x}^N,f,\alpha)$ and Eqs. (7) and (19), where $\alpha$ is defined below. The $N!$ in Eq. (29) is required because with the HS reconstruction the atoms are not labeled.

It should be noted that because $f$ is small and the future cells are positioned differently from one rebuilding step to another with respect to the previously placed atoms, the related thermodynamic system is not a usual *homogeneous* grand canonical system; therefore, the chemical potential $\mu$, and the temperature appearing in Eqs. (22)–(28) might be different from the corresponding bulk values. In fact, the optimal values of these quantities are those that minimize the approximate entropy $S^A(f,\alpha)$ [Eq. (7)] or in turn maximize the corresponding free energy $F^A(f,\alpha)$ [Eq. (8)]. More specifically, because $T$, $\mu$, and $\Lambda$ always appear in the equations as multiples of $\exp[\mu/k_BT]/\Lambda^3$, we fix $\Lambda$ using the simulation temperature $T$ [the "true" thermodynamic temperature that appears in $F=E-TS^A$, e.g., Eqs. (4), (8), and (20)], and use this $T$ also in $\exp[\mu/k_BT]$. On the other hand, $\mu$ and the temperature denoted $T_p$ in the equations above are optimized. As $f$ is increased one would expect $T_p$ and $\mu$ to approach their bulk values. Moreover, we have found that assigning individual parameters $\mu_i$ to different partition function terms (e.g., $Q_1^j$) decrease $S^A$ dramatically; these parameters define the set denoted by $\alpha$ in Eqs. (5)–(15).

## III. RESULTS AND DISCUSSION

### A. The systems studied and the approximations applied

We present results for argon obtained with the boundary conditions BC4, which are suitable for a continuum liquid and are easy to program. Spiral boundaries, on the other hand, are inappropriate because they are likely to impose undesired repulsions among the image and boundary atoms. We have studied the system at four different densities and temperatures. The two highest reduced densities, $\rho^*=N\sigma^3/V=0.846$ and 0.75 (see Table I), correspond to liquid argon, and those for 0.5 and 0.1 correspond to what we loosely describe as a supercritical fluid and a dense gas, respectively. We have chosen these values in order to cover a large range of conditions and to compare our results with those obtained with other methods. The densities, temperatures, box and cell lengths, and the number of cells appear in Table I; also presented in the table is $\rho_{\text{cell}}$, the number of atoms $N$ (i.e., the number of occupied cells) divided by the total number of cells, which is ~0.3 for $\rho^*=0.846$. Most of the calculations were performed for $N=216$ atoms, however, in order to check the effect of the boundary conditions we also studied a significantly larger system of $N=1728$ atoms.

Five HS approximations were applied, based on $f=1-4$ future cells, where for $f=1$ only the target cell was considered while for $f>1$ some or all of its nearest neighbor cells were taken into account as well. In every case, all $f$ singlets were taken into account and an approximation is therefore denoted by $f/d$, where $d$ is the number of doublets considered. Notice that creation of triplets in $f=4$ adjacent cells is very unlikely because the corresponding $\rho_{\text{cell}}=0.75$ constitutes a large fluctuation already for the highest density studied, $\rho_{\text{cell}}=0.3$; therefore, the effect of triplets is ignored. Obviously, if $f$ is increased to 5 or 6, the $\rho_{\text{cell}}$ value of triplets decreases to 0.6 and 0.5, respectively, and their effect becomes important. We carried out a preliminary study using $f>4$ where the effect of triplets was taken into account, and thus verified the potential for this higher approximation to improve the results. The computer time increased significantly, however, and we decided for now not to perform a systematic study. In the best approximation presented here, 4/6 all of the possible four singlets and six doublets were taken into account. Another parameter that affects the approximation is the number of cubes (subcells) $l=b\times b\times b$. We applied $b=3$, 4, and 5 and found, as one would expect, that in most cases $b=5$ has led to the best results, i.e., to the smallest entropy, $S^A$ [Eq. (7)]. In the other few cases we attribute the slightly smaller $S^A$ obtained for $b=3$ or 4 to an incorrect treatment of the atomic repulsions by these relatively crude meshes.

Initially, we generated samples of argon systems of $N=216$ and 1728 atoms at different densities and temperatures (see Table I) under (standard) periodic boundary conditions using the Metropolis MC method; in all cases the Lennard-Jones interactions were truncated at 10.8 Å (which is half of the box length of the $N=216$ system with the highest density, see Table I). With this procedure at each MC step an atom is selected at random, a trial random move is generated within a small Cartesian cube around the atom position, and the move is accepted or rejected according to the usual MC criterion; the cube (step) size was adjusted to obtain an acceptance rate of ~0.5. After every $500N$ MC steps the current configuration was recorded for a future analysis, which has led to uncorrelated samples as indicated by the calculated autocorrelation functions of the energy and entropy. It should

TABLE II. Comparison between the optimal parameters $T_p$ and $\mu_1$ and their thermodynamic counterparts, $T$ and $\mu$, for the approximation 1/0.[a]

| $\rho^*$ | $T$ (K) | $T$ (K) | $-\mu_1$ (kcal/mol) | $-\mu$ (kcal/mol)[a] |
|---|---|---|---|---|
| 0.846 | 96.71 | 96.53 | 2.12 | 2.21 |
| 0.75 | 125.76 | 137.77 | 2.78 | 2.75 |
| 0.5 | 175.50 | 161.73 | 3.10 | 3.46 |
| 0.1 | 123.18 | 126.74 | 2.68 | 2.79 |

[a]The results for $\mu$ are presented up to the second decimal place; their statistical errors are much smaller.

be pointed out that the long-range (tail) correction[19] has been added to the energy of each sampled configuration.

### B. Optimization of parameters

The first stage of the HS implementation is the optimization of the temperature parameter $T_p$ and the chemical potential parameters, $\mu_i$ that were assigned to each singlet and doublet, thus, totaling 11 for the best approximation, 4/6. These parameters were optimized gradually by a simple Monte Carlo procedure applied initially to the (repeated) reconstruction of one configuration, and followed by refinement cycles based on five and twenty configurations. For the highest approximation this procedure runs typically overnight on a 2 GHz PC; less time is needed for the lower approximations. The optimal set of $\mu_i$ and $T_p$, i.e., those that minimize the entropy functional $S^A$, are used in the HS production runs. We have found that for all of the approximations studied the maximal deviation of the optimized $T_p$ values from the corresponding thermodynamic temperature $T$ is by 11%. The different $\mu_i$ values obtained for a given approximation deviate from their average by up to 17%. In Table II results are presented for $\mu_i$ and $T_p$ obtained for all of the densities for the approximation 1/0. The thermodynamic chemical potential values provided in the table were calculated from the pressure and the free energy obtained from thermodynamic integration runs (see Appendix). It is evident that the parameters $\mu_i$ deviate from their thermodynamic counterparts, $\mu$ by no more than 10%.

### C. The free energy fluctuations

In Table III results are displayed for the free energy functional per atom, $A_c/\epsilon N(F^A)$ [Eq. (21)] and its fluctuation, $\sigma^A$ [Eq. (14)] for three cases, $\rho^*=0.846$ and $N=216$, $\rho^*=0.846$ and $N=1728$, and $\rho^*=0.75$ and $N=216$, for five approximations. As expected, in all cases $A_c/\epsilon N(F^A)$ that is the lower bound of the correct free energy, increases systematically as the approximation improves. Also, the $A_c/\epsilon N(F^A)$ results for $N=1728$ are only slightly smaller, by no more than 0.003, than their counterparts obtained for $N=216$. This is important, meaning that the effect of the boundary conditions already for $N=216$ is small. For good enough approximations, the fluctuations are expected to decrease as the approximation improves, which is materialized for $\rho^*=0.75$ but is only satisfied for approximations 1–3 of $\rho^*=0.846$. The latter results probably stem from the fact that the fluctuations are insensitive to the relatively small decrease, by 0.02 and 0.007 in the values of $A_c/\epsilon N(F^A)$ in going from approximation 3 to 4 and from 4 to 5, as compared to the larger decrease of 0.084 and 0.074 between approximation 1 and 2 and 2 and 3, respectively. For $\rho^*=0.75$ the decrease of $A_c/\epsilon N(F^A)$ by 0.043 between approximation 3 to 4 is relatively large, and the fluctuation of approximation 4 is therefore significantly smaller than that of approximation 3; this probably reflects the fact that a better HS approximation is defined for $\rho^*=0.75$ than for $\rho^*=0.846$.

Therefore, to analyze the correlation between the results of the free energy and its fluctuation [Eq. (15)] one should consider only results with decreasing fluctuations such as those for approximations 1, 2, and 4, or 1, 2 and 5, for $\rho^*=0.846$. In Table IV we display the best-fit results based on Eq. (15), which were obtained from the appropriate results of Table III. It should be pointed out again that the best-fit function should be concave down, i.e., the exponent $\beta$ should be larger than 1. This condition has not been met for most of the results for $\rho^*=0.75$ and for 1, 2, and 5 for $\rho^*=0.846$ ($N=216$). The table reveals that $A_c/\epsilon N(F^{\mathrm{up}})$ which is the intersection of the tangent to the curve with the ordinate, as expected, is always an upper bound. The corresponding averages, $A_c/\epsilon N(F^{M2})$ [Eq. (16)], and the extrapolated values, $A_c/\epsilon N(F^{\mathrm{extp}})$ for each system are relatively spread but their average is equal within the error bars to the value obtained by thermodynamic integration (TI), which is considered to be correct.

TABLE III. Results for the free energy functional $A_c/\epsilon N(F^A)$ [Eqs. (8) and (21)] and its fluctuation, $\sigma^A$, for different approximations.[a]

| Approx. No. | Approx. | $\rho^*=0.846$ $N=216$ | | $\rho^*=0.846$ $N=1728$ | | $\rho^*=0.75$ $N=216$ | |
|---|---|---|---|---|---|---|---|
| | | $-A_c/\epsilon N(F^A)$ | $\sigma^A$ | $-A_c/\epsilon N(F^A)$ | $\sigma^A$ | $-A_c/\epsilon N(F^A)$ | $\sigma^A$ |
| 1 | 1/0 | 4.5305 | 0.0416 | 4.5320 | 0.0144 | 3.9346 | 0.0439 |
| 2 | 2/1 | 4.4470 | 0.0376 | 4.4490 | 0.0134 | 3.8724 | 0.0392 |
| 3 | 3/2 | 4.3729 | 0.0324 | 4.3753 | 0.0120 | 3.8153 | 0.0337 |
| 4 | 4/3 | 4.3532 | 0.0326 | 4.3558 | 0.0120 | 3.7720 | 0.0321 |
| 5 | 4/6 | 4.3464 | 0.0331 | 4.3492 | 0.0120 | 3.7662 | 0.0317 |
| | TI | 4.120(1) | | 4.1298(7) | | 3.645(1) | |

[a]$\rho^*$ are $N$ are defined in Table I. The statistical errors of the free energy and the fluctuations, $\sigma^A$ [Eq. (14)] are smaller than $\pm 0.0005$. The statistical errors of the TI results appear in parentheses, e.g., $4.120(1)=4.120 \pm 0.001$.

TABLE IV. Upper bound and extrapolated values for $A_c/\epsilon N$ based on the correlation between $A_c$ and $\sigma^A$ [Eqs. (14)–(16)].[a]

| Approx. | $-A_c/\epsilon N(F^{\mathrm{up}})$ | $-A_c/\epsilon N(F^{M2})$ | $-A_c/\epsilon N(F^{\mathrm{extp}})$ | $-A_c/\epsilon N(\mathrm{TI})$ |
|---|---|---|---|---|
| | | $\rho^*=0.846$ $N=216$ | | |
| 1,2,3 | 4.024 | 4.199 | 4.292 | |
| 1,2,4 | 3.784 | 4.069 | 4.064 | |
| Average | | | 4.16(6) | 4.120(1) |
| | | $\rho^*=0.846$ $N=1728$ | | |
| 1,2,3 | 3.919 | 4.147 | 4.303 | |
| 1,2,4 | 3.669 | 4.012 | 4.163 | |
| 1,2,5 | 3.538 | 3.943 | 4.025 | |
| Average | | | 4.10(5) | 4.1298(7) |
| | | $\rho^*=0.75$ $N=216$ | | |
| 1,2,3 | 3.513 | 3.664 | 3.709 | |
| 3,4,5 | 3.256 | 3.511 | 3.731 | |
| Average | | | 3.65(5) | 3.645(1) |

[a]$F^{\mathrm{up}}$ stands for the upper bound of $F$ [Eq. (16)], $F^{M2}$ denotes the average free energy [Eq. (16)], $F^{\mathrm{extp}}$ is the extrapolated free energy [Eq. (15)], and TI stands for the free energy obtained by thermodynamic integration that is considered to be exact. The values in the forth column and the rows denoted ''average'' are averages of the related free energy results denoted $F^{M2}$ and $F^{\mathrm{extp}}$. The notation for the errors is defined in the caption of Table III.

### D. Results for the entropy and the free energy

As discussed earlier, upper bounds for the free energy can also be obtained by $F^B$ [Eqs. (9) and (10)], and indeed, reliable results for $A_c/\epsilon N(F^B)$ were obtained for the low density systems of $\rho^*=0.75$, 0.5, and 0.1, where the HS approximation improves; as expected, the corresponding values of the acceptance rate $R$ [Eq. (12)], 1.4%, 3.9%, and 8.9%, increase as well. Notice that while $R=1.4\%$ is relatively low, it stems from a single low free energy configuration that appeared in the beginning of the process. However, by calculating block averages of the results for $A_c/\epsilon N(F^B)$ we have verified that the result for $\rho^*=0.75$ is statistically reliable. The results for $A_c/\epsilon N(F^B)$ appear in Table V.

Table V summarizes the various results for the free energy for $N=216$, providing thereby a comparison of our approximations with the TI values. It should first be pointed out that for $\rho^*=0.1$ the results were obtained for the lowest approximation 1/0 (based on the target cell only) because the better approximations did not improve the results. For $\rho^*=0.846$, 0.75, 0.5, and 0.1 the $A_c/\epsilon N(F^A)$ values underestimate the correct ones by no more than 5.5%, 3.3%, 0.9%, and 0.6%, respectively. The corresponding minimal deviations of $A_c/\epsilon N(F^{M1})$ (and for $\rho^*=0.846$ and 0.75 the deviations of the average results obtained in Table IV that are denoted in Table V by an asterisk) are 1.4*%, 1.6% (1.4*%), 0.26%, and 0.25%. We also provide free energy results for argon obtained by others, which are close to our TI values; however, the highest density and temperature in these studies, $\rho^*=0.835$ and $T^*=0.81$ are slightly different from our values $\rho^*=0.846$ and $T^*=0.806$.

Table VI displays results for the excess entropy, $S_e$ [Eq. (19)], and for completeness also the corresponding results for the excess free energy, $F_e/T$ [Eq. (20)] and the average potential energy $E/T$. In this representation the deviations of the HS results from the correct values increase as compared to those obtained by $A_c$ in Table V. Thus, the minimum deviations of the $F^A$ values are 7%, 5.5%, 2.1%, and 4.3% for $\rho^*=0.846$, 0.75, 0.5, and 0.1, respectively, whereas the corresponding deviations of $F^M$ are, 1.9*%, 2.5% (2.4*%), 0.5%, and 1.4%. The errors of the entropy are larger than their free energy counterparts, increasing to 7.9%, 4%, 1.6%, and 4.7% for $S^A$, and to 2.2*%, 1.9% (1.8*%), 0.5%, and 1.3% for $S^M$, for $\rho^*=0.846$, 0.75, 0.5, and 0.1, respectively. As expected $E/T$ and $S_e$ both increase as the density decreases.

To study the effect of the boundary conditions on the free energy, we carried out calculations for $N=216$ and

TABLE V. Results for the free energy, $A_c$ [Eq. (21)] of an argon system of 216 atoms.[a]

| $\rho^*=N\sigma^3/V$ | $-A_c/\epsilon N(F^A)$ | $-A_c/\epsilon N(F^B)$ | $-A_c/\epsilon N(F^M)$ | $-A_c/\epsilon N(\mathrm{TI})$ | $-A_c/\epsilon N$ (others) |
|---|---|---|---|---|---|
| 0.846 | 4.346 | | 4.16 (6)* | 4.120(1) | 4.15(2)[b] |
| | | | | | 4.17(3)[c] |
| | | | | | 4.10(4)[d] |
| 0.75 | 3.766 | 3.641(5) | 3.704(3) | 3.645(1) | 3.67(2)[b] |
| | | | 3.65 (5)* | | 3.64(3)[c] |
| | | | | | 3.65 (a)[e] |
| 0.5 | 3.839 | 3.790(3) | 3.815(2) | 3.805(1) | 3.83(2)[b] |
| | | | | | 3.79(3)[c] |
| | | | | | 3.85(2)[e] |
| 0.1 | 3.995 | 3.967(3) | 3.981(2) | 3.971(1) | 3.96(2)[b] |
| | | | | | 3.97 (3)[f] |

[a]The HS approximation is the same, $f/d=4/6$ for the first three densities and 1/0 for $\rho^*=0.1$; the sample size in all cases is 5000 configurations. The $F^B$ results are based on Eqs. (10) and (11), leading to the corresponding $F^M$ results [$F^M=F^{M1}$, see Eq. (13)]. Results for $F^M$ appearing with an asterisk are those denoted ''average'' in Table IV. TI are the thermodynamic integration results. The statistical errors for $A_c/\epsilon N(F^A)$ are smaller than $\pm 0.0005$ (see Table III). The notation for the errors is defined in the caption of Table III.
[b]Reference 26.
[c]Reference 24.
[d]Reference 27.
[e]Reference 25.
[f]Reference 23.

TABLE VI. Results for the energy, entropy, and the free energy of an argon system with 216 atoms.[a]

| | | $-S_e$ [cal/(K mol)] | | | $-F_e/T$ [cal/(K mol)] | | |
|---|---|---|---|---|---|---|---|
| $P^*$ | $-E/T$ [cal/(K mol)] | $S^A$ | $S^M$ | TI | $F^A$ | $F^M$ | TI |
| 0.846 | 14.798 (1) | 6.364(3) | 6.82(15)* | 6.923(4) | 8.430 (2) | 7.97(15)* | 7.875(3) |
| 0.75 | 8.8279(4) | 4.848(2) | 4.953(6) | 5.056(3) | 3.981 (1) | 3.875(6) | 3.772(2) |
| 0.75 | 8.8279(4) | | 5.05 (9)* | 5.056(3) | | 3.78 (9)* | 3.772(2) |
| 0.5 | 4.9730(5) | 2.655(2) | 2.689(4) | 2.703(2) | 2.3181(5) | 2.284(3) | 2.270(2) |
| 0.1 | 1.758 (2) | 0.784(3) | 0.810(5) | 0.829(3) | 0.9715(4) | 0.948(4) | 0.929(2) |

[a]$E$ is the average Lennard-Jones potential energy [Eq. (20)], $S_e$ is the excess entropy [Eq. (19)], and $F_e$ is the excess free energy [Eq. (20)]. $S^A$ is based on Eq. (7), with $\rho_i(f,\alpha)$ replacing $P_i(f,\alpha)$. The results for $S^A$ and $F^A$ are based on the best HS approximations for each density. $S^M$ is obtained from $(E-F^M)/T$, where $F^M$ is defined by $F^{M1}$ [Eq. (13)] and when the results appear with an asterisk by $F^{M2}$ [Eq. (16)] (see also the caption of Table V). TI denotes the thermodynamic integration results.

$\rho^*=0.846$ with the boundary conditions BC3 discussed earlier. We applied BC3 with different levels of approximation. One, applied to 4/3 is based on eight parameters ($T_p$ and seven $\mu_i$) only, whereas with the best approximation altogether 83 parameters were defined by assigning different $\mu_i$ to different boundary regions of the box. These two treatments have led to $A_c/\epsilon N(F^A)=-4.546$. and $-4.484$, respectively, which constitutes a significant increase in the free energy for the better approximation. This demonstrates the strong effects of the boundaries in the BC3 treatment for small systems. Still $A_c/\epsilon N(F^A)=-4.484$ is significantly lower than $-4.346$ obtained with BC4 (see Table V). However, as discussed earlier, a better treatment of BC3 would make the calculation highly complex. The BC3 treatment of the boundaries is expected to improve as the system size increases, which indeed is demonstrated by the significantly higher value $A_c/\epsilon N(F^A)=-4.476$ obtained with the 4/3 approximation (with eight parameters) for 1728 atoms as compared to $-4.546$ obtained for 216 atoms.

## IV. SUMMARY AND CONCLUSIONS

In this article we have extended for the first time the hypothetical scanning method to a fluid system. It has been demonstrated that by considering only four future cells very good results can be obtained for a large range of argon densities, where even for the highest density studied the error of $A_c$ is $\sim$1.4%, of $F_e/T$ is $\sim$1.9% and that of the access entropy, $S_e$ is $\sim$2.2%. A HS analysis of 5000 configurations based on dividing the cell into $b^3=4^3$ cubes requires $\sim$6 h CPU on a 2 GHz Athlon processor; this time increases to $\sim$35 h for $b=5$; for comparison, the TI calculation described in the Appendix required $\sim$4 h CPU. It should be pointed out that the HS analysis is especially suitable for parallel computing where each processor treats a partial configuration, a single or several configurations. The method can systematically be improved by considering two or three additional future cells, where, however, treating the time consuming triplets is required; as discussed above, this can be carried out efficiently on a computer cluster that at this point is not available for us. An efficient handling of the triplets might be achieved by replacing the systematic future scanning by a Monte Carlo integration procedure, where positions in the future cells are selected at random, as carried out before within the framework of the double scanning method.[59] For good enough approximations the HS method provides upper and lower bounds for the free energy, and in particular it is suitable for treating large systems. Still, we consider the present study as an initial development of the HS approach for liquids. Thus, in the following article we describe a different implementation of the HS ideas, where the calculation of the transition probabilities is based not on calculating future partition functions, but on simulating future configurations by the Monte Carlo method and counting the population of the target cell and the target cube of interest. We expect both implementations to further be improved as they applied to the more complex models of water.

## ACKNOWLEDGMENTS

This work was supported by NIH Grant No. 7R01 GM61916-02 and partially by NIH Grant No. 1R01 GM66090-01.

## APPENDIX: FREE ENERGY CALCULATIONS USING THERMODYNAMIC INTEGRATION

Most of the free energy values for Lennard-Jones fluids in the literature are relatively old hence of limited accuracy. An exception is the more recent extensive work of the Gubbins group, which enables one to determine the free energy numerically from a polynomial expression of the equation of state based on 33 adjustable parameters that were fitted to a large amount of simulation data.[60] However, we have found it beneficial to obtain values for comparison that exactly match the systems and the simulation/running conditions used by us to study HS. Therefore, we calculated highly accurate results for the free energy and entropy of the present systems independently using a version of thermodynamic integration (TI), which is described here in some detail; the reader is also referred to several review articles,[1–4] where a wider scope of this approach is given.

With TI the free energy of a liquid of given $NVT$ can be obtained by integrating the change in the free energy in going from an ideal gas with the same $NVT$ (the reference state) to the liquid of interest. Thus a coupling parameter, $\lambda$, is added to the potential energy, which allows one to define a nonphysical path connecting the reference state ($\lambda=0$) to the liquid state ($\lambda=1$),

$$E(\mathbf{x}^N,\lambda)=\sum_{i<j}\phi(r_{ij},\lambda), \tag{A1}$$

where $\phi(r_{ij},\lambda)$ is the scaled Lennard-Jones pair potential, becoming $\phi(r_{ij})$ [Eq. (17)] for $\lambda=1$ and 0 for $\lambda=0$. Because the partition function can be formally written as a function of $\lambda$, the derivative of the Helmholtz free energy can be evaluated as an ensemble average,

$$\frac{\partial F}{\partial\lambda}=\left\langle\frac{\partial E(\mathbf{x}^N,\lambda)}{\partial\lambda}\right\rangle_\lambda. \tag{A2}$$

The change in the Helmholtz free energy is therefore given by

$$\Delta F=\int_0^1\frac{\partial F}{\partial\lambda}d\lambda, \tag{A3}$$

where the integration is approximated as a quadrature over a discrete number of derivative points. Here, each derivative at $\lambda_i$ is obtained from a simulation of the respective scaled system at $\lambda_i$.

From a practical point of view, the particular path chosen (i.e., the scaling form) can strongly influence the reliability of the results. For example, in scalings involving the creation of atoms, small but energetically acceptable pair separations, at one value of $\lambda$, can correspond to very high repulsive energies for slightly larger $\lambda$. This gives rise to very high (and variable) values for the derivative, thus causing difficulties in the integration process (the ''van der Waals end point catastrophe''). Therefore, we have used a shifted scaling potential, introduced by Zacharias *et al.*,[61]

$$\phi(r_{ij},\lambda)=\lambda 4\epsilon\left[\frac{\sigma^{12}}{(r_{ij}^2+\delta(1-\lambda))^6}-\frac{\sigma^6}{(r_{ij}^2+\delta(1-\lambda))^3}\right], \tag{A4}$$

where the shift parameter, $\delta$, prevents divergence in the potential (and its derivative) at small pair separations. $\delta$ is generally kept fixed along the path. Other efficient scalings/integrations are available, see for example, Ref. 62.

The scaled system was simulated at 41 evenly spaced values of $\lambda$ using the standard Metropolis MC method in the canonical $(N,V,T)$ ensemble. Each simulation was run to a total of $5\times10^6$ MC steps ($10^7$ for 1728 atoms). The pair interactions were truncated at 10.8 Å. Formally, we added the long-range corrections to the ensemble-averaged derivatives. (The integrated contribution of these derivative corrections is trivially equivalent to the long-range energy correction at $\lambda=1$.) The quadrature accounted for curvature, in that triplets of successive derivative points were fitted to piecewise quadratic functions (two of these piecewise quadratics can be averaged between each pair of points, except at the ends). The derivatives were generally very smooth, and simple trapezium integrations (i.e., the derivative function is taken as linear between each point) typically gave free energy changes that were different from the piecewise quadratic quadrature by only 0.05% or less. Uncertainty values in the ensemble-averaged derivatives were calculated from the standard deviation of block averages. These uncertainties were used in a standard error propagation (assuming a trapezium integration) to estimate the uncertainty in the over all free energy change. These uncertainty estimates are reasonably consistent with observed differences in independent runs. Though we have chosen to integrate over a large number of $\lambda$ values (simulation points), very good results can be obtained with far fewer values. On the systems we checked, the results for 11 and 21 $\lambda$ values agree (with 41) within the calculated uncertainties.

Reliable integration results can usually be obtained with a shift parameter value of 9 Å$^2$ (which generally promotes a very smooth quadrature). This choice can however give rise to negative pressures. This has never caused problems with the 216-atom system. However, a collapse (phase transition) was observed in the 1728 atom system using this $\delta$ value. To avoid negative pressures, $\delta$ can be reduced or alternatively, the integration can be carried out at a higher temperature. The free energy at the desired temperature is then obtained from another integration (over $T$), using the derivative, $\partial(F/T)/\partial(1/T)=E$. Results from this alternative path are consistent within the calculated uncertainty.

As a further check on our values, we also integrated the free energy using a series of microcanonical $(N,V,E)$ MD simulations over a physical path of $(p,V,T)$ points ($p$ is the pressure and here $E$ is the total energy). This path is started from a dilute gas at $T=200$ K (assumed ideal), and thus the free energy is analytically evaluated. $V$ and $E$ are varied (point by point) over the path, which ultimately ends at the liquid state of interest. As $V$ is decreased, $E$ is changed in such a way that $T$ stays close to 200 K (i.e., above the critical temperature), thus avoiding the crossing of a phase transition. After the liquid density has been reached, $E$ is lowered to achieve the desired $T$. $p$ and $T$ are ensemble averaged at each $(p,V,T)$ point (a total of 112 simulations). The entropy change, from the analytically calculable ideal gas to the liquid state, is integrated over the path as

$$\Delta S=\int_{\text{path}}\left[\frac{1}{T}dE+\frac{p}{T}dV\right], \tag{A5}$$

where the first (most dilute) simulation started at a pressure of ~10 atm and a small correction to the entropy was added using the second virial coefficient for argon. The procedure was carried out for a system of 216 atoms at the liquid state, $\rho^*=0.846$, $T=96.53$ K. The results for the configurational Helmholtz free energy [Eq. (21)] obtained from this approach and the potential scaling approach agree to within less than 0.1%.

[1] D. L. Beveridge and F. M. DiCapua, Annu. Rev. Biophys. Biophys. Chem. **18**, 431 (1989).
[2] P. A. Kollman, Chem. Rev. **93**, 2395 (1993).
[3] W. L. Jorgensen, Acc. Chem. Res. **22**, 184 (1989).
[4] H. Meirovitch, in *Reviews in Computational Chemistry*, edited by K. B. Lipkowitz and D. B. Boyd (Wiley, New York, 1998), Vol. 12, p. 1.
[5] N. Metropolis, A. W. Rosenbluth, M. N. Rosenbluth, A. H. Teller, and E. Teller, J. Chem. Phys. **21**, 1087 (1953).
[6] B. J. Alder and T. E. Wainwright, J. Chem. Phys. **31**, 459 (1959).
[7] J. A. McCammon, B. R. Gelin, and M. Karplus, Nature (London) **267**, 585 (1977).
[8] N. Gō and H. A. Scheraga, J. Chem. Phys. **51**, 4751 (1969).
[9] N. Gō and H. A. Scheraga, Macromolecules **9**, 535 (1976).
[10] A. T. Hagler, P. S. Stern, R. Sharon, J. M. Becker, and F. Naider, J. Am. Chem. Soc. **101**, 6842 (1979).

[11] M. Karplus and J. N. Kushick, Macromolecules **14**, 325 (1981).
[12] J. Schlitter, Chem. Phys. Lett. **215**, 617 (1993).
[13] H. Schäfer, A. E. Mark, and W. F. van Gunsteren, J. Chem. Phys. **113**, 7809 (2000).
[14] H. Schäfer, X. Daura, A. E. Mark, and W. F. van Gunsteren, Proteins **43**, 45 (2001).
[15] I. Andricioaei and M. Karplus, J. Chem. Phys. **115**, 6289 (2001).
[16] I. R. MacDonald and K. Singer, J. Chem. Phys. **47**, 4766 (1967).
[17] J.-P. Hansen and L. Verlet, Phys. Rev. **184**, 151 (1969).
[18] W. G. Hoover and F. H. Ree, J. Chem. Phys. **47**, 4873 (1967).
[19] M. P. Allen and D. J. Tildesley, *Computer Simulation of Liquids* (Clarenden, Oxford, 1987).
[20] J. G. Kirkwood, J. Chem. Phys. **3**, 300 (1935).
[21] R. W. Zwanzig, J. Chem. Phys. **22**, 1420 (1954).
[22] D. R. Squire and W. G. Hoover, J. Chem. Phys. **50**, 701 (1969).
[23] G. M. Torrie and J. P. Valleau, Chem. Phys. Lett. **28**, 578 (1974).
[24] G. M. Torrie and J. P. Valleau, J. Comput. Phys. **23**, 187 (1977).
[25] D. Levesque and L. Verlet, Phys. Rev. **182**, 307 (1969).
[26] Z. Li and H. A. Scheraga, J. Phys. Chem. **92**, 2633 (1988).
[27] E. M. Gosling and K. Singer, Pure Appl. Chem. **22**, 303 (1970); J. Chem. Soc., Faraday Trans. 2 **69**, 1009 (1973).
[28] A. M. Ferrenberg and R. H. Swendsen, Phys. Rev. Lett. **63**, 1195 (1989).
[29] S. Kumar, J. M. Rosenberg, D. Bouzida, R. H. Swendsen, and P. A. Kollman, J. Comput. Chem. **16**, 1339 (1995).
[30] B. Berg and T. Neuhaus, Phys. Lett. B **267**, 249 (1991); Phys. Rev. Lett. **68**, 9 (1992).
[31] A. P. Luybartsev, A. A. Martsinovski, S. V. Shevkunov, and P. N. Vorontsov-Velyaminov, J. Chem. Phys. **96**, 1776 (1992).
[32] W. P. Reinhardt, M. A. Miller, and L. M. Amon, Acc. Chem. Res. **34**, 607 (2001).
[33] F. Wang and D. P. Landau, Phys. Rev. Lett. **86**, 2050 (2001).
[34] M. S. Shell, P. G. Debenedetti, and A. Z. Panagiotopoulos, www.arXiv.org: cond-mat/03/05210 (2003).
[35] H. Meirovitch, Chem. Phys. Lett. **45**, 389 (1977).
[36] H. Meirovitch, J. Stat. Phys. **30**, 681 (1983).
[37] H. Meirovitch, Phys. Rev. B **30**, 2866 (1984).
[38] H. Meirovitch, M. Vásquez, and H. A. Scheraga, Biopolymers **26**, 651 (1987).
[39] H. Meirovitch, S. C. Koerber, J. Rivier, and A. T. Hagler, Biopolymers **34**, 815 (1994).
[40] C. Baysal and H. Meirovitch, Biopolymers **50**, 329 (1999).
[41] Z. R. Wasserman and F. R. Salemme, Biopolymers **29**, 1613 (1990).
[42] S. K. Ma, *Statistical Mechanics* (World Scientific, Singapore, 1985).
[43] A. J. Chorin, Phys. Fluids **8**, 2656 (1996).
[44] A. J. Chorin, *Vorticity and Torbulence* (Springer-Verlag, Berlin, 1994).
[45] A. J. Schilijper and B. Smit, J. Stat. Phys. **56**, 247 (1989).
[46] H. Meirovitch, J. Chem. Phys. **111**, 7215 (1999).
[47] H. Meirovitch, J. Phys. A **16**, 839 (1983).
[48] H. Meirovitch, Phys. Rev. A **32**, 3709 (1985).
[49] H. Meirovitch and H. A. Scheraga, J. Chem. Phys. **84**, 6369 (1986).
[50] H. Meirovitch, J. Chem. Phys. **97**, 5816 (1992).
[51] H. Meirovitch, J. Chem. Phys. **114**, 3859 (2001).
[52] Z. Alexandrowicz, J. Chem. Phys. **55**, 2765 (1971).
[53] H. Meirovitch and Z. Alexandrowicz, J. Stat. Phys. **16**, 121 (1977).
[54] R. Kikuchi, Phys. Rev. **81**, 988 (1951).
[55] H. Meirovitch, J. Phys. A **115**, 2063 (1982).
[56] An alternative point of view: One could ''cut out'' a square (cubic) section of a *very large* reconstructed system and use the product of the TPs from just the ''cut out'' portion to calculate the per-atom entropy of this portion. This entropy will become exact for a very large system when the ''cut out'' portion is also large.
[57] T. L. Hill, *Statistical Mechanics Principles and Selected Applications* (Dover, New York, 1956).
[58] H. Meirovitch and Z. Alexandrowicz, J. Stat. Phys. **15**, 123 (1976).
[59] H. Meirovitch, J. Chem. Phys. **89**, 2514 (1988).
[60] J. K. Johnson, J. A. Zollweg, and K. E. Gubbins, Mol. Phys. **78**, 591 (1993).
[61] M. Zacharias, T. P. Straatsma, and J. A. McCammon, J. Chem. Phys. **100**, 9025 (1994).
[62] M. Mezei, Mol. Simul. **2**, 201 (1989).